The Therapeutic Nanobody Profiler: characterising and predicting nanobody developability to improve therapeutic design

Gemma L. Gordon [1], João Gervasio [1,2], Colby Souders [3], and Charlotte M. Deane [1,✉]

[1]Department of Statistics, University of Oxford, Oxford, UK; [2]Model-Based Evolutionary Genomics Unit, Okinawa Institute of Science and Technology Graduate University, Okinawa, Japan; [3]Twist Bioscience, South San Francisco, California, US

Developability optimisation is an important step for successful biotherapeutic design. For monoclonal antibodies, developability is relatively well characterised. However, progress for novel biotherapeutics such as nanobodies is more limited. Differences in structural features between antibodies and nanobodies render current antibody computational methods unsuitable for direct application to nanobodies. Following the principles of the Therapeutic Antibody Profiler (TAP), we have built the Therapeutic Nanobody Profiler (TNP), an open-source computational tool for predicting nanobody developability. Tailored specifically for nanobodies, it accounts for their unique properties compared to conventional antibodies for more efficient development of this novel therapeutic format. We calibrate TNP metrics using the 36 currently available clinical-stage nanobody sequences. We also collected experimental developability data for 108 nanobodies and examine how these results are related to the TNP guidelines. TNP is available as a web application at *opig.stats.ox.ac.uk/webapps/tnp*.

Correspondence: ***deane@stats.ox.ac.uk***

Introduction

The design of a successful biologic drug requires the optimisation of properties beyond the ability to bind to a target. Candidates must also demonstrate favourable developability: the capacity of a molecule to undergo manufacture, storage and transport whilst retaining its function [1, 2]. Developability encompasses properties such as solubility, stability, yield, and aggregation propensity, all of which impact the viability of a potential therapeutic. For instance, poor expression can hinder scalability, whereas aggregation may drive unwanted immunogenicity [3].

Antibodies, the largest class of biologic drugs [4], have well-established experimental methods for assessing developability. Techniques such as size exclusion chromatography (SEC), cross-interaction chromatography (CIC) or hydrophobic interaction chromatography (HIC) are used to assess the extent of aggregation or aggregation propensity, which may arise from non-specific binding or hydrophobicity [1, 5, 6]. Susceptibility to non-specific binding can be further tested via baculovirus (BVP) ELISA [1]. Light-based methods such as affinity-capture self-interaction nanoparticle spectroscopy (AC-SINS) and dynamic light scattering (DLS) serve to identify self-association and quantify polydispersity, which can lead to challenges in formulation [7, 8]. Melting and aggregation temperatures (Tm and Tagg) indicative of thermal stability can be measured using differential scanning fluorimetry (DSF) [9].

Reliable *in silico* approaches have the potential to streamline antibody development by reducing time-consuming and costly bench work [10, 11]. Computational tools for antibody developability prediction have emerged in recent years leveraging sequence and structural data, often alongside *in vitro* assays [1, 12–17]. Machine learning models have increasingly been applied to antibody developability prediction [18–20] and multi-parameter optimisation [21–24].

Whilst the simultaneous optimisation of multiple developability properties remains challenging [22], several tools assess these properties in parallel. For example, the Therapeutic Antibody Profiler (TAP) scores developability based on five surface and structural features which are benchmarked against clinically-tested therapeutics [2]. These metrics include descriptors for surface hydrophobicity and charge, and for CDR loop characterisation. Building on this, Ahmed *et al.* (2021) [25] determined a physicochemical profile for the variable regions of marketed biotherapeutics and compared this profile with the characteristics of candidate antibodies. Similarly, Park and Izadi (2024) have proposed six descriptors for electrostatic surface properties and hydrophobicity for antibody developability prediction, examining how these correlate with experimentally-determined properties [26]. Most recently, Bashour *et al.*. (2024) [27] extended this approach, computing a total of 86 sequence and structure-based descriptors in order to map developability 'landscapes' for antibodies.

Existing studies on developability have focused primarily on monoclonal antibodies. As a result, efforts towards *in silico* prediction for novel formats such as nanobodies remain sparse, with the few examples centred around library design or optimisation of a

single property [28–30]. Computational tools designed for conventional antibodies are usually not directly applicable to nanobodies due to their distinct structural features [11]. For example, nanobodies have no light chain, existing as a single domain. They show a tendency towards longer CDR3 loops, which allows for a broader range of possible conformations [31, 32]. In addition, the exposed framework 2 (FR2) region contains conserved nanobody tetrad residues which enhance solubility and stability - this feature is not observed in conventional antibodies, since the FR2 region is typically buried by the variable light chain domain [31]. These characteristics affect not only antigen binding [33] but also the biophysical properties of the nanobody, and thus their developability.

In this work, we characterise the structural properties of nanobodies in the context of developability, conducting a comparative analysis with clinical-stage nanobodies and experimental developability data. Our results reveal structural diversity among clinical-stage nanobodies, suggesting that developability is not constrained to a narrow subset of their conformational space. In order to further explore nanobody developability, we experimentally tested 108 clinical stage and proprietary nanobodies for properties such as aggregation, polyspecificity, self-association and thermostability. We assess the relationship between *in silico* and *in vitro* developability assessments.

Based on this analysis, we have built the Therapeutic Nanobody Profiler (TNP), a developability predictor tailored to nanobodies that follows the framework of the Therapeutic Antibody Profiler (TAP) [2]. TNP enables the comparison of predicted structures against 36 clinical-stage nanobodies to inform the design of developable nanobodies. TNP will be updated as clinical-stage data grows over time, enabling increasingly robust evaluations of developability. The web application is publicly available at *opig.stats.ox.ac.uk/webapps/tnp*.

Methods

Sequence data

Non-redundant sequence datasets were obtained from the TheraSAbDab [34], Observed Antibody Space (OAS) [35, 36], PLAbDab-nano [37] and SAbDab [38, 39] databases to represent nanobody diversity across clinical-stage data, natural immune repertoires, patents, publications, and crystal structures (**Table 1**).

Clinical-stage data was obtained from TheraSAbDab, including sequences at any trial stage and including bi- and multi-specifics, for which each different variable domain is counted separately. Natural sequences for antibody VH chains and VHHs respectively were obtained from studies by Jaffe *et al.* 2022 [40] and Li *et al.* (2016) [41] and extracted from OAS. To support structure prediction with a feasible dataset size, a single file was selected from these datasets and smaller representative sets were randomly sampled from the non-redundant sequences. The data from PLAbDab-nano were split into three datasets by source, dividing sequences from patents, published literature and crystal structures (which are collected from SAbDab [38, 39]). The final dataset used in this work is comprised of 72 proprietary VHH sequences from Twist Bioscience.

Dataset	Total
Clinical-stage Nbs	36
Clinical-stage antibody VH	919
Natural Nbs	4059
Natural antibody VH	2047
Nb patents	563
Nb literature	410
Nb crystal structures	738
Nb proprietary	72

Table 1. The total sequences and modelled structures in each dataset. Full lists of the non-proprietary sequences can be found at *github.com/oxpig/TNP*.

Structural data

Predicted structures were generated for all sequence datasets using NanoBodyBuilder2 [42] for nanobody data, and HeavyBuilder2, a modified version of ABodyBuilder2 (ABB2) [42], for antibody VH sequences.

HeavyBuilder2 uses the same architecture as ABB2 and a similar dataset of crystal structures for training, curated from SAbDab [38, 39]. While the ABB2 training data ensured that structures had both VH and VL chains, for HeavyBuilder2 the VL was removed from the dataset. The validation data included the VH chain of 49 antibodies from the Rosetta Antibody Benchmark. The test set was the same as that used to benchmark ABB2: all Fv region files added to SAbDab between the 1st of August 2021 and the 1st of June 2022. Three deep-learning models were independently trained for the prediction of antibody VH chains. The best prediction was selected by aligning predicted structures and choosing the one with the closest CDR-H3 conformation to the average of the three predictions. By default, HeavyBuilder2 passes the prediction through a structural refinement step.

For pairwise comparison of the CDR3 conformations of known crystal structures, 76 pairs of bound and unbound nanobodies were curated from SAbDab. A list of the Protein Data Bank (PDB) IDs for these pairs is given in the Supplementary Information (**Table S1**).

Numbering schemes

The IMGT numbering scheme and CDR definitions were used throughout this work (CDR1: IMGT residues 27-38, CDR2: IMGT residues 56-65, CDR3: IMGT residues 105-117) [43]. The nanobody 'tetrad'

or hallmark residues refer to residues at positions 42, 49, 50 and 52 on the FR2 region. ANARCI [44] was used to number sequences for the annotation of CDR3 loops and hallmark residues.

Computed descriptors for developability properties

Patches of surface hydrophobicity and charge were calculated following methods from TAP [2]. A range of additional developability-related sequence and structural properties were calculated following methods from Bashour *et al.* (2024) [27], with a Python implementation of the associated code which is available at *github.com/oxpig/TNP*. A full list of the properties included grouped by class according to Bashour *et al.* can be found in **Table S2**.

Describing CDR3 loop conformations

The conformations of the CDR3 loops were analysed according to a spherical coordinate system, following methods in Gordon *et al.* (2023) [33]. The CDR3 loop is described by its 'compactness', defined as the reach of the CDR3 loop away from the rest of the variable domain, divided by its length (number of residues). A loop with lower compactness reaches away from the variable domain, whereas a loop of higher compactness is folded against the variable domain.

We compared this to the classification of CDR3 conformations as either 'kinked' or 'extended', following methods in Weitzner *et al.* (2015) and Bahrami-Dizicheh *et al.* (2023) [45, 46]. This classification is based on the τ pseudo-dihedral and α angles between backbone Cα atoms in the CDR3 at positions 116, 117 and 118 (by IMGT numbering). Kinked loops have α and τ angles in the range: $0° < \alpha116 < 120°$, $85° < \tau116 < 130°$. Extended loops have α and τ angles in the range: $-100° > \alpha116$, $100° < \tau116 < 145°$ (**Figure S1**).

Interactions between the CDR3 loop and nanobody tetrad residues

Arpeggio (v1.4.1) [47] was used to analyze interatomic interactions between pairs of residues from the CDR3 loop and nanobody tetrad. Structures were hydrogenated for this analysis using gemmi v0.6.7 [48], following methods in Bashour *et al.* (2024) [27].

Visualization

All visualizations were created using open-source PyMOL v2.4.1 [49], logomaker v0.8[50], and matplotlib v3.7.0 [51].

In vitro developability assays

In vitro assays for developability were carried out on 108 nanobody sequences: 36 derived from clinical-stage data, with the remaining 72 from Twist proprietary data.

Analytical Size Exclusion Chromatography (aSEC). Size-exclusion chromatography (SEC) was used to evaluate the molecular size distribution and structural integrity of protein samples, including detection of monomer content, aggregation, and degradation. Approximately 5 µg of each protein sample was injected onto an Advance Bio SEC column (300 Å, 4.6 × 150 mm, 2.7 µm particle size; Cat. # PL1580-3301, Agilent Technologies) pre-equilibrated with phosphate-buffered saline (PBS) (Cat. #BP399-20; Fisher Scientific).

The separation was carried out on an Agilent 1260 Infinity II HPLC system using PBS as the mobile phase at a flow rate of 0.35 mL/min. Elution was monitored by UV absorbance at 280 nm. Since the separation is based on hydrodynamic volume, larger protein species elute earlier, while smaller species elute later.

Chromatograms were analysed using Agilent Chem Station Open Lab CDS software. Peak retention times and areas were used to assess the proportion of monomeric protein as well as the presence of high molecular weight aggregates or low molecular weight degradation products.

Cross Interaction Chromatography (CIC). The CIC assay was employed to assess the propensity of a test protein to bind non-specifically to immobilized proteins (commonly human IgG) which serves as an indicator of aggregation risk. To construct the CIC column, approximately 30 mg of polyclonal human antibodies (I4506; Sigma) are covalently bound to a 1-mL NHS-activated HiTrap column (17-0716-01; Cytiva), followed by quenching with ethanolamine (Cat # 104679; Carterra). For each run, around 5 µg of antibody is injected, and phosphate-buffered saline (PBS) is used as the mobile phase, flowing at 0.1 mL/min on an Agilent 1260 Infinity II HPLC system. Chromatographic data are acquired and analysed using Agilent Chem Station Open Lab CDS software.

Hydrophobic Interaction Chromatography (HIC). The HIC assay was performed to evaluate the relative hydrophobicity of antibody samples, which can be indicative of developability risks such as aggregation and nonspecific interactions [1, 52] The assay was conducted using a Proteomix HTC Butyl-NP5 column, 4.6 × 100 mm (Cat. #431NP5-4610; Sepax Technologies).

Antibody samples (5 µg at 1 mg/mL) were diluted with mobile phase A (1.8 M ammonium sulfate (Cat. # J64419.A3; Thermo Scientific) and 0.1 M sodium phosphate (Cat. #S373-500; Fisher Scientific, Cat. #S468-500; Fisher Scientific), pH 6.5) to achieve a final ammonium sulfate concentration of 1 M prior to injection. Chromatographic separation was performed using a linear gradient elution over 20 minutes, transitioning from mobile phase A to mobile phase B (0.1

M sodium phosphate, pH 6.5) at a flow rate of 1.0 mL/min. UV absorbance was monitored at 280 nm using an Agilent 1260 Infinity II HPLC system. Retention times were determined using Agilent Chem Station Open Lab CDS software.

Dynamic Light Scattering (DLS). Protein particle size distribution and solution homogeneity were characterised using dynamic light scattering (DLS). Each protein sample was loaded into standard capillaries (Cat. # PR-AC002; Nano Temper Technologies) with an approximate volume of 10 µL and analysed using the Prometheus Panta instrument. Sample-specific details including identity, buffer conditions, and concentration were entered into the software platform (PR Panta Analysis, Version 1.9) before measurements were initiated. DLS measurements yielded two principal values: the hydrodynamic radius (rH) and the polydispersity index (PDI). The rH reflects the average diffusion-based size of particles in solution, indicative of the protein's physical state.

Nano Differential Scanning Fluorimetry (nDSF). Samples were introduced into the Prometheus Panta system (Nano Temper Technologies) using standard capillaries (Cat. # PR-AC002; Nano Temper Technologies) with a loading volume of approximately 10 µL. Prior to measurement and data acquisition, sample metadata including identification, concentration, and buffer composition were recorded using the system's control software (PR Panta Analysis, Version 1.9).

An initial discovery scan was conducted to optimise excitation parameters by determining the appropriate light intensity tailored to the optical characteristics of each sample. Following this calibration step, thermal unfolding experiments were performed by gradually increasing the temperature from 15℃ to 95℃ at a constant ramp rate of 1℃ per minute. Fluorescence signals were captured simultaneously at 330 nm and 350 nm throughout the scan to monitor temperature-dependent changes in protein conformation. The ratio of fluorescence intensity at 350 nm to 330 nm (F350/F330) was plotted against temperature. Transitions in structural conformation were identified as inflection points in the curve, with the first deviation from baseline indicating the onset of unfolding (Tonset). The point of maximum slope, derived from the first derivative of the fluorescence ratio curve, was used to determine the thermal transition midpoint (Tm).

Affinity-capture Self-interaction Nanoparticle Spectroscopy (AC-SINS). To evaluate the self-interaction potential of protein candidates, the AC-SINS assay was carried out following previously established protocols [1]. Gold nanoparticles (Cat. #15705, Ted Pella Inc.) were prepared by coating with a mixture of antibodies: 80% anti-human IgG Fc-specific goat antibody (Cat. #109-005-098, Jackson ImmunoResearch) and 20% non-specific goat polyclonal antibody (Cat. #005-000-003, Jackson ImmunoResearch). These coated particles serve as a capture surface for test proteins via Fc-mediated interactions. Protein samples were incubated with the functionalized nanoparticles for 2 hours at room temperature. Following incubation, spectral absorbance was recorded using an Agilent Biotech Epoch Microplate Spectrophotometer reader, and data were analysed. A shift in the peak absorbance wavelength relative to the mouse IgG or PBS control was interpreted as a signature of particle aggregation caused by antibody self-association.

BVP ELISA. The assay procedure was adapted from the protocol described by Jain *et al.* (2017) [1]. In summary, baculovirus particles (Cat. # E3001;Medna Scientific) were prepared by mixing viral stock with 50 mM sodium carbonate buffer (pH 9.6) in 1:200 dilution and applied to 384 well ELISA plates (Cat. #464718;Thermo Scientific). Plates were incubated overnight at 4℃ to allow coating. The following day, unbound particles were removed by aspiration, and all subsequent steps were performed at room temperature. Wells were blocked with 75 µL of PBS containing 2% BSA for 1 hour, followed by three washes with PBS (75 µL per well). Test antibodies, diluted to 100 µg/mL in blocking buffer (25 µL), were then added to each well and incubated for 1 hour. Plates were washed six times with PBS before the addition of 25 µL of HRP-conjugated Goat Anti Human IgG, Fcy sp. secondary antibody (Cat. # 115-035-098; Jackson Immuno Research), followed by another 1-hour incubation. After a second series of six washes with PBS, 25 µL of TMB substrate (Cat. # 5120-0083; Sera Care) was added, and the reaction allowed to proceed for 10–15 minutes. The enzymatic reaction was stopped with 25 µL of 2 M sulfuric acid, and absorbance was measured at 450 nm using an Agilent Biotech Epoch Microplate Spectrophotometer reader. To calculate the BVP score, absorbance values were normalized to wells containing no test antibody.

Results

We first examine the structural differences between antibody VH chains and nanobodies that are likely to impact developability, initially investigating the TAP metrics that can be directly applied to nanobodies (total CDR length and patches of surface hydrophobicity, positive charge, and negative charge across the CDR vicinity) and then more nanobody-specific features, including CDR3 loop conformation and hallmark residues (the nanobody tetrad). This leads to a list of six metrics for use in the TNP. We next calibrate these metrics using the 36 currently available clinical-stage nanobody sequences, and a set of 72 proprietary nanobodies for which we collected *in vitro* developability data, including assessments for non-specific binding (using a CIC assay), polyspecificity (BVP-ELISA), hydrophobicity (HIC), self-association (AC-SINS) and aggregation (DLS).

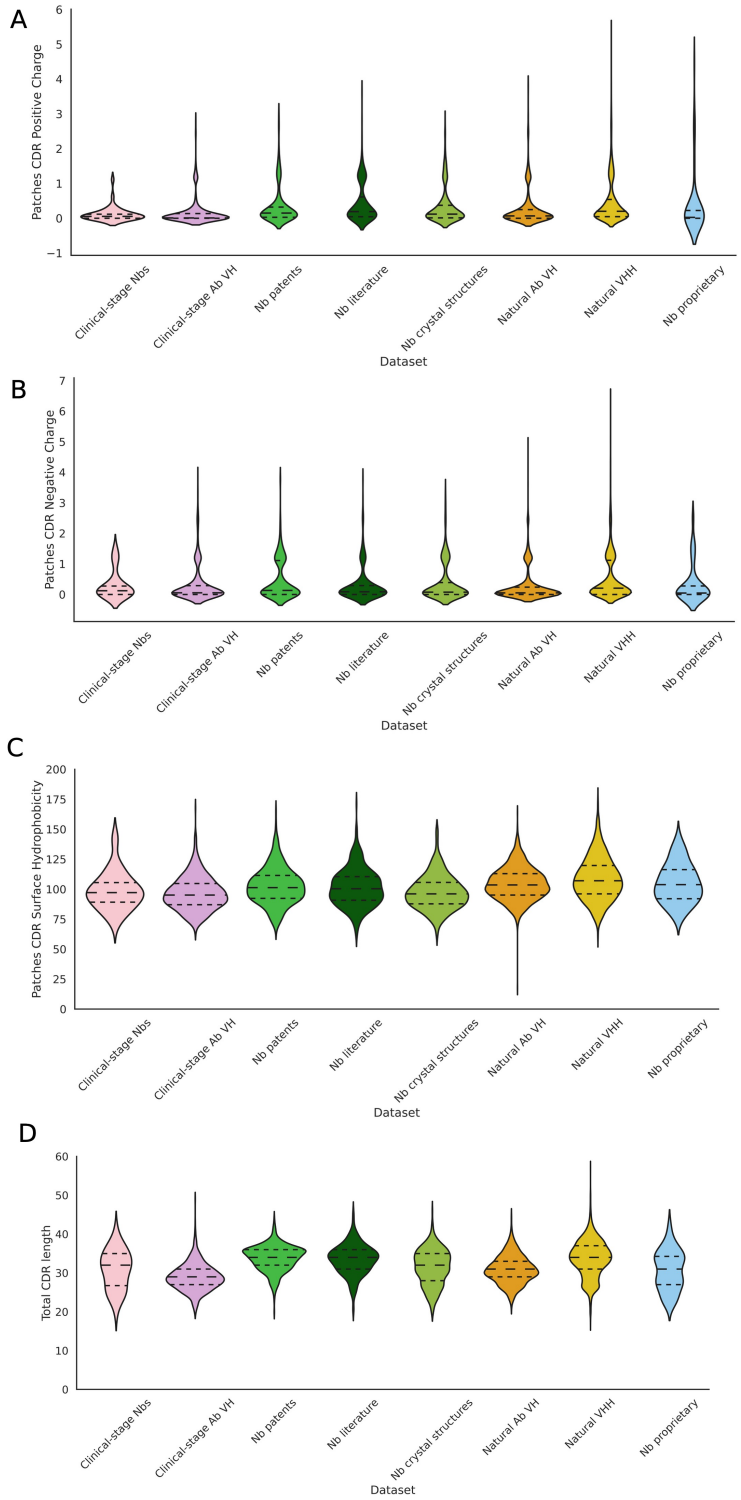

Figure 1. Distributions of the TAP metrics on our 8 datasets of nanobodies and antibody VH chains from different sources. The TAP metrics score candidates on (**A**) patches of positive charge, (**B**) patches of negative charge, (**C**) patches of surface hydrophobicity and (**D**) total CDR length. The clinical-stage nanobody data show distinctions from antibody VH data and nanobodies from a range of other sources.

Distributions of the TAP metrics differ between antibody and nanobody clinical data

To assess whether clinical-stage nanobodies occupy distinct ranges across the applicable TAP metrics, the distributions of these metrics were computed across our datasets on sequences and predicted structures (**Figure 1**). We compared clinical-stage nanobodies to those from natural immune repertoire data, structures, and publications and patents, as well as to antibody VH domains from both natural and clinical-stage sources.

Clinical-stage nanobodies have a more constrained range for patches of positive and negative charge, than any other dataset (**Figure 1A, B**, **Figure S2, S3**). For patches of surface hydrophobicity, the range for clinical-stage nanobodies largely overlaps with the other datasets (**Figure 1C**, **Figure S4**).

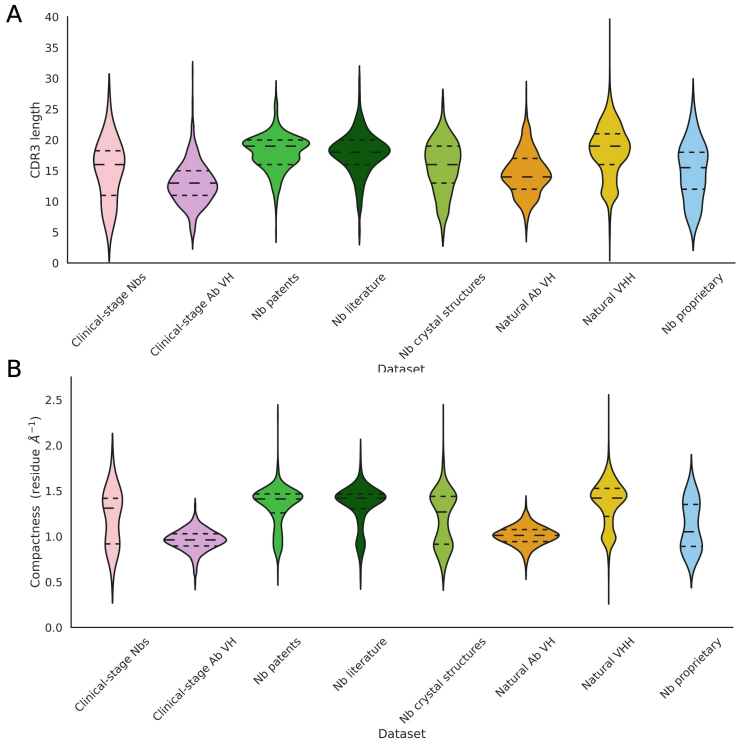

Figure 2. Distributions of the CDR3 length and CDR3 compactness on our 8 datasets of nanobodies and antibody VH chains from different sources. **(A)** Clinical-stage nanobodies occupy a wide range of CDR3 lengths. **(B)** The CDR3 loop conformation can be described using compactness, a measure of the loop reach relative to its length. Nanobodies, including the clinical-stage data, show a bimodal distribution for compactness, representing two clusters of loop conformations.

Total CDR length tends to be higher for all nanobody datasets than the antibody VH datasets, though the range for clinical-stage nanobodies is more limited than in the natural VHH data and even the clinical-stage antibody VH data (**Figure 1D**, **Figure S5**). The difference between the nanobody and antibody datasets is most likely due to the longer CDR3 in nanobodies.

Total CDR length does not sufficiently capture nanobody paratope shapes

In TAP, the total CDR length measure for antibodies is a strong indicator of both the length of the heavy chain CDR3 and the paratope shape. As nanobodies typically have a longer CDR3 than antibodies [33, 53–56] and do not have a light chain, they have a greater diversity of CDR3 conformations [31, 32, 54], meaning that this measure may not capture CDR3 conformation. We investigate the relationship between CDR3 conformation (and therefore paratope shape) and loop length in nanobodies, in particular looking at whether CDR3 length or total CDR length captures CDR3 compactness (see **Methods**).

Compactness is a measure of loop reach normalized for loop length (**Figure S6**). We selected compactness as our descriptor for CDR3 conformation as this provides a continuous scale with which to describe CDR3 conformations (**Figure S7**, **Figure S8**). Our continuous measure of compactness more precisely captures the diversity of loop conformations than previous methods ([32, 45, 46], **Figure S9**), whilst remaining consistent with their overall classification system (**Figure S10**, **Figure S11**).

Lower compactness corresponds to the CDR3 extending upward like an antibody CDR-H3 constrained by a VL chain, whereas higher compactness scores indicate that the loop folds down over the FR2 region [33]. Previous work has shown that the CDR3 of nanobodies have a bimodal distribution of compactness, whilst antibody CDR-H3 loops do not [33], suggesting that a compactness measure may be needed for a nanobody profiler.

In our datasets, clinical-stage nanobodies tend to show a relatively balanced distribution of CDR3 length (in terms of number of residues), including shorter CDR3 loops not typically seen in natural, patented, or literature-derived nanobodies (**Figure 2A**, **Figure S12**). The CDR3 length profiles of the clinical-stage, proprietary, and crystal structures sets of nanobodies align most closely with clinical-stage VH domains, suggesting the presence of more VH-like features.

As expected, our nanobody datasets show a bimodal distribution of compactness, while the antibody VH data do not (**Figure 2B**, **Figure S13**). Clinical-stage nanobodies appear to show the presence of two subpopulations of CDR3 conformations, which is not captured by total CDR length or CDR3 length alone, indicating that the inclusion of CDR3 compactness in the TNP metrics would help capture the nanobody paratope shape. These results also suggest that nanobody developability is not limited to either of the compactness subpopulations.

More compact CDR3 loops do not show significant conformational change upon binding

A large proportion of nanobodies with longer CDR3 loops show higher compactness scores (**Figure S11**). To determine whether there is a conformational change happening upon binding to allow these compact loops to extend out, a set of 76 pairs of bound and unbound crystal structures were curated (see **Methods**, **Table S1**) to allow pairwise comparison of CDR3 conformation and compactness.

Compactness scores are consistent between bound and unbound nanobody structures (**Figure 3**). Any observed changes in compactness are minimal, and there is no correlation between the change in compactness and the root mean square deviation (RMSD) over the bound and unbound CDR3 loops (which indicates any discrepancy between the crystal structures) (**Figure S14**). This suggests that a conformational change, where a more compact loop unfolds and extends out from the FR2 region, is unusual.

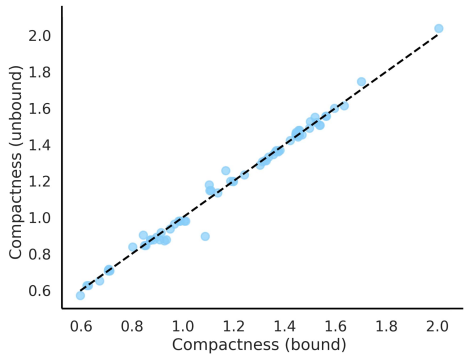

Figure 3. Pairwise comparison of compactness scores for bound and unbound nanobody crystal structures suggests that the CDR3 loop does not undergo a significant conformational change upon binding.

Nanobody subtypes based on CDR3 loop conformations show associated tetrad motifs

Previous studies have described interactions between the CDR3 loop and nanobody tetrad residues present on the exposed FR2 surface [46, 57–60]. These residues are critical to surface hydrophobicity and solubility and thus affect developability [60].

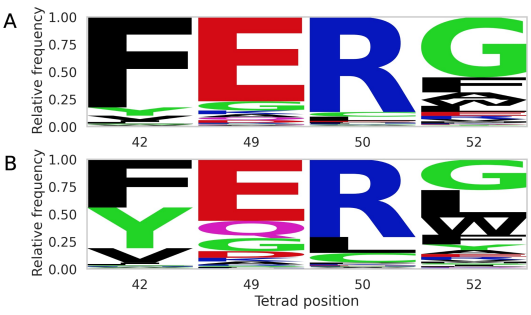

Figure 4. Amino acid frequencies across the nanobody tetrad positions (42, 49, 50 and 52 by IMGT numbering) in nanobodies shows greater variation per position in loops of lower compactness versus higher compactness. (**A**) Logo plot of amino acid frequencies in loops of higher compactness. (**B**) Logo plot of amino acid frequencies in loops of lower compactness.

We observe that canonical nanobody tetrad motifs, such as FERG or FERG-like motifs, are predominant across nanobodies, while VGLW is most common in antibody VH chains (**Figure S15**), supporting the existing literature [58]. Among nanobodies, those with higher compactness tend to retain these classically nanobody-like motifs. Loops with lower compactness display greater diversity in tetrad motifs (**Figure 4**). The tetrad motif is therefore a useful metric to include in the TNP, as it can help stratify nanobodies into distinct structural subtypes.

Hydrophobic interactions between aromatic residues often occur between nanobody tetrad residues and more compact CDR3 loops

Between pairs of CDR3 and nanobody tetrad residues, hydrophobic, aromatic and carbon-π interactions are the most common [60] (**Figure S16**). For CDR3 loops of higher compactness, we found that the most common interacting amino acids are between aromatic residues such as phenylalanine, which is highly conserved at position 42 in the nanobody tetrad, and a second aromatic residue in the CDR3 loop (**Figure 5**, **Figure S17**).

The necessity of these interactions for structural stability in longer loops folded over the FR2 region makes the identities of these tetrad residues, alongside the CDR3 conformation, an important consideration for the design of developable molecules. This supports the inclusion of the tetrad motif and CDR3 compactness in the TNP, as the co-optimisation of these properties may lead to improved developability.

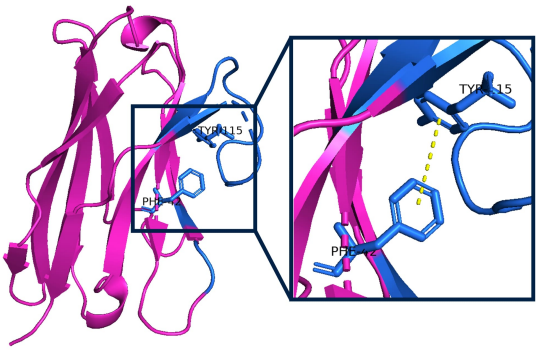

Figure 5. Hydrophobic interactions between aromatic residues in the CDR3 loop and the first nanobody tetrad position (IMGT position 42), here between a tyrosine and phenylalanine, occur often in a more compact CDR3 loop which tends to be folded over the FR2 region. The framework region is shown in pink and the CDR loops and tetrad residues are shown in blue.

In vitro assays support the presence of two equally developable nanobody subtypes

Developability assays (including aSEC, CIC, HIC, BVP-ELISA, AC-SINS, DLS and DSF) were carried out on a set of 108 nanobody sequences, including 36 clinical-stage sequences, with the remainder comprised of proprietary candidates from Twist Bioscience (see **Methods**).

Metric	Range	Amber flag region	Amber flag threshold	Red flag region	Red flag threshold
Total CDR length	20-39	Top 5%, bottom 5%	20-24, 37.25-39	Above or below	<20, >39
CDR3 length	5-23	Top 5%, bottom 5%	5-8, 21.25-23	Above or below	<5, >23
CDR3 compactness	0.56-1.61	Top 5%, bottom 5%	0.56-0.81, 1.57-1.61	Above or below	<0.56, >1.61
PSH	73.40-155.47	Top 5%, bottom 5%	73.40-79.59, 126.83-155.47	Above or below	<73.40, >155.47
PPC	0.00-1.18	Top 5%	0.39-1.18	Above	>1.18
PNC	0.00-1.88	Top 5%	1.47-1.88	Above	>1.88

Table 2. Flagging thresholds for TNP are set according to distributions of 36 nanobody clinical-stage data-points.

The data were divided into groups of lower and higher compactness (using a threshold score of 1.25 as per **Figure S7**), a proxy to distinguish between the two subpopulations. Across all assay results, the range of values for nanobodies of lower and higher compactness are largely comparable (**Figure S18**). Although some candidates within these ranges exhibit poorer scores and may be less developable, the primary conclusion is that there is no need to bias selection toward either nanobody subtype.

TNP properties

Based on the above analysis, we have selected six properties for use in TNP: total CDR length, CDR3 length, CDR3 compactness, and patches of surface hydrophobicity, positive charge and negative charge across the CDR vicinity. These are aimed at capturing the major sequence and structural features that will influence developability. In order to assess how well these features represent the data, we calculated a further 81 surface and structural properties for our nanobody datasets following the methods described in Bashour *et al.* [27]. We make this data publicly available at *github.com/oxpig/TNP*. These properties were correlated alongside the original TAP metrics and the additional descriptors introduced in TNP to assess their redundancy (**Figure S19**). Overall, our results indicate that our selected six metrics are a sensible small set of interpretable descriptors that avoid redundancy. However, there are many other choices that could be made.

Developability guidelines for TNP are set by 36 clinical-stage nanobody sequences and predicted structures

For our chosen metrics, clinical-stage nanobodies show distributions distinct from antibody clinical data or nanobody non-clinical data. We defined thresholds for our developability guidelines based on the 36 clinical-stage nanobodies (**Table 2**). Following the TAP methodology, an amber flag is assigned where a nanobody scores within the lowest and/or highest 5% of a distribution, and a red flag is assigned where properties lie outside the current observed clinical range. These thresholds will be updated as new candidates progress through clinical trials.

In vitro and *in silico* methods provide complementary approximations of developability

We performed *in vitro* assays (including aSEC, CIC, HIC, BVP-ELISA, AC-SINS, DLS and DSF, see **Methods**) for developability properties on a set of 108 nanobody sequences, comprising 36 clinical-stage sequences and 72 proprietary candidates from Twist Bioscience (for which one failed to express). We evaluated the proprietary sequences against our TNP metrics to determine their positioning relative to the clinical thresholds. These predictions were then compared against their *in vitro* assay data, in which five assays (CIC, HIC, BVP-ELISA, AC-SINS and DLS) were scored using the same green–amber–red flagging system as the computational metrics. Thresholds for these flags were derived based on the range of scores across all 108 VHHs in the panel.

The proprietary candidates predominantly fall within the range defined by the clinical-stage nanobodies (**Figure 6**). No red flags were observed for surface hydrophobicity patches, whilst they most frequently occurred for patches of positive charge. In total, 14 red flags were identified across 11 proprietary candidates (**Table 3**). Of these, only one candidate exhibited multiple red flags - the remaining ten each had a single red flag.

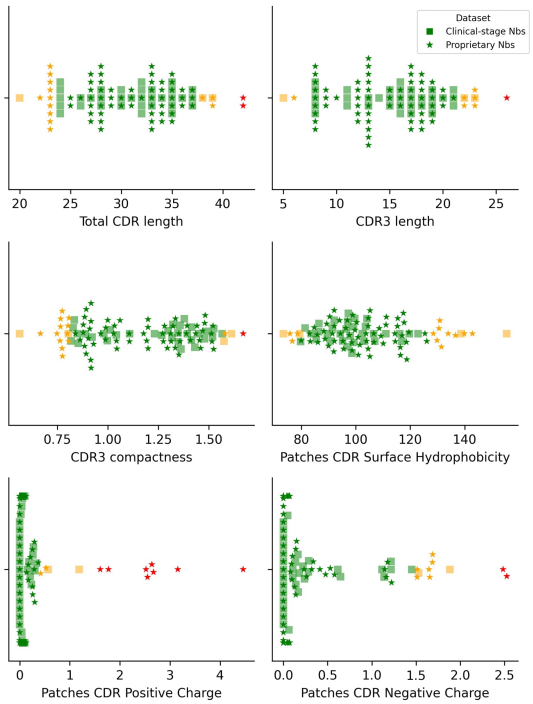

Figure 6. Distributions of values for each TNP metric for nanobody clinical-stage and proprietary data, coloured by flags assigned according to thresholds set by the clinical-stage data. Data points in red highlight proprietary candidates that fall outside the current observed guidelines.

Sample	Total CDR length	CDR3 length	CDR3 compactness	Patches CDR Surface Hydrophobicity	Patches CDR Positive Charge	Patches CDR Negative Charge	CIC Retention Time (min)	HIC Retention Time (min)	BVP-ELISA OD450 (a.u.)	AC-SINS Δλmax (nm)	DLS PDI
1	42	23	1.58	136.61	0.01	1.51	9.48	20.19	0.96	4.57	0.34
2	42	26	1.67	142.86	4.46	0.09	8.80	17.56	3.22	1.79	0.18
3	34	18	1.36	95.27	3.16	0.23	9.43	12.91	2.77	3.60	0.85
4	39	23	1.51	139.88	1.77	0.58	9.13	12.95	0.84	6.78	0.31
5	39	23	1.52	130.88	1.61	0.34	9.20	14.85	0.23	8.65	0.24
6	36	20	1.47	114.50	0.42	2.48	9.20	17.29	0.34	3.68	0.16
7	36	20	1.48	125.41	0.21	2.53	9.59	23.14	1.48	6.52	0.13
8	35	18	1.11	126.08	2.64	0.06	10.74	23.60	2.51	17.56	0.80
9	35	18	1.03	118.59	2.55	0.05	10.30	20.50	1.75	19.88	0.87
10	35	18	1.11	111.10	2.67	0.07	9.79	17.40	0.82	14.18	0.98
11	35	18	1.06	117.49	2.52	0.06	10.33	20.70	1.81	18.13	0.88

Table 3. Comparison of proprietary candidates from Twist Bioscience that were assigned red flags by TNP against *in vitro* assay data demonstrates that *in silico* and *in vitro* measures provide different approximations for developability. Values are coloured according to the TNP flags for the TNP metrics, derived from the ranges seen for these metrics across the 36 clinical-stage nanobodies. The *in vitro* assay values were assigned flags according to thresholds set by the ranges observed across all 108 nanobodies assayed.

For candidates flagged as high-risk by TNP, there is agreement with *in vitro* assay outcomes, where all those with red flags for at least one TNP metric also show at least one amber flag for the *in vitro* assays, with most showing multiple amber and red flags (**Table 3**). For example, Sample 2 was assigned red flags for total CDR length, CDR3 length, CDR3 compactness and patches of positive charge. This is accompanied by amber flags for patches of surface hydrophobicity and the HIC assay, as well as a red flag in the BVP-ELISA assay. Upon manual inspection, this structure has a very long, compact CDR3 loop, which can increase the likelihood of it containing larger, more hydrophobic residues to interact with the FR2 region [46] and may potentially lead to increased non-specific binding which is captured by the BVP-ELISA [61]. A similar pattern is observed for Sample 1, with consistent signals across both predicted and experimental metrics.

Some candidates display discrepancies between TNP predictions and *in vitro* assay results. Apart from red flags for patches of positive or negative charge, samples 7-11 receive green flags across all other TNP metrics. However, their *in vitro* assay data show multiple amber or red flags, often across all five assays, suggesting very poor developability profiles. A similar pattern is observed among the 36 clinical-stage nanobodies: although these molecules have advanced to clinical trials and therefore must to some extent achieve acceptable developability, many still receive amber or red flags in the *in vitro* assays (**Table S3**). Relatively weak correlations between our calculated computational metrics and *in vitro* assay data suggest that there is limited agreement across all 108 experimentally-tested nanobodies and is not specific to our chosen metrics (**Figure S20**).

Web application

TNP is available as a web application at *opig.stats.ox.ac.uk/webapps/tnp*. Users can input a nanobody sequence to generate a developability profile. The computed metrics include patch scores for surface hydrophobicity, positive charge, and negative charge, as well as total CDR length, CDR3 length, and CDR3 compactness. Each continuous metric is benchmarked against a reference distribution derived from 36 clinical-stage nanobody sequences and predicted structures, with green, amber, or red flags assigned accordingly.

The web application enables visualization of the nanobody structure with mapped surface patches for hydrophobic and charged regions. Additionally, it provides annotations of the tetrad residues and highlights potential sequence liabilities exposed on the nanobody surface.

Discussion

In this paper, we introduced the Therapeutic Nanobody Profiler, a developability predictor specifically designed to account for the unique structural features of nanobodies, extending the methodology established by the Therapeutic Antibody Profiler (TAP) [2].

Our analysis demonstrates that clinical-stage nanobodies show distinct features compared to both clinical-stage and natural antibodies, supporting the need for a nanobody-specific developability tool. We find that nanobody CDR3 diversity is less constrained than in antibody therapeutics, with clinical-stage nanobodies spanning the full range of CDR3 lengths, including longer loops not typically observed in monoclonal antibodies [33, 53–56].

Whilst these CDR3 loops adopt diverse conformations, they cluster into two structural subtypes based on compactness, our description of the loop length relative its reach. The first subtype has generally longer, more compact loops (which fold over the FR2 region) and classical VHH-like tetrad motifs. Hydrophobic interactions between pairs of tetrad residues and CDR3 residues are common in these cases. The second subtype tends towards shorter, VH-like loops that extend away from the framework, with greater variation in the tetrad residue identities. Our findings are consistent with previous observations identifying distinct kinked and extended conformations in VHH CDR3 loops and stabilising interactions between the CDR3 loop and tetrad residues in kinked conformations [46, 58–60].

Both of these subtypes of CDR3 compactness are present in the clinical-stage nanobody data, indicating that both are developable. These results suggest that therapeutic design need not be biased towards a particular conformational subtype. However, these subtypes may also impose design limitations: as longer CDR3 loops tend to fold over the FR2 region for stability, a compromise between CDR3 loop reach and length may be required to design a convex paratope that can reach less accessible epitopes. In the Therapeutic Antibody Profiler (TAP), total CDR length was used to capture both CDR3 length and paratope shape [2]. Total CDR length alone does not fully capture the more complex characteristics of the nanobody CDR3 loop, and so in the TNP, we include additional metrics for CDR3 length and compactness, to better describe the unique features we have observed.

As more nanobodies progress through clinical trials, the thresholds for the Therapeutic Nanobody Profiler will be adjusted, strengthening the reliability of developability predictions made using the software. Alongside the web application, we provide the Python package for high-throughput analyses as well as the first publicly available set of nanobody developability assay data, and extensive datasets of computational descriptors calculated for the nanobodies analysed in this study. These resources aim to facilitate the development of nanobody-specific computational tools and support new hypotheses for the successful design of therapeutic nanobodies.

Data availability

The web application is publicly available at *opig.stats.ox.ac.uk/webapps/tnp*. The Python package is available at *github.com/oxpig/TNP*. This GitHub repository also contains the *in vitro* assay data for the 108 clinical-stage and proprietary nanobodies, sequence data for the datasets analysed here (excluding the proprietary sequences), the corresponding data for their TNP values and 81 other computational descriptors, and the code used to calculate these descriptors.

Acknowledgements

We extend thanks to Matthew Raybould and the co-authors of the original Therapeutic Antibody Profiler [2]. This work was supported by the Engineering and Physical Sciences Research Council (grant number EP/S024093/1) and Twist Bioscience.

Author contributions

CD conceptualized and designed the study. CD and CS supervised the project. GG carried out the data curation and analysis. JG developed structure prediction methods used for data generation. The manuscript was written by GG, with contributions from JG, and reviewed by CD and CS. All authors contributed to the article and approved the submitted version.

References

1. Jain, T. *et al.* Biophysical properties of the clinical-stage antibody landscape. *Proceedings of the National Academy of Sciences* **114,** 944–949. https://doi.org/10.1073/pnas.1616408114 (2017).
2. Raybould, M. I. J. *et al.* Five computational developability guidelines for therapeutic antibody profiling. *Proceedings of the National Academy of Sciences* **116,** 4025–4030. https://doi.org/10.1073/pnas.1810576116 (2019).
3. Zhang, W. *et al.* Developability assessment at early-stage discovery to enable development of antibody-derived therapeutics. *Antibody Therapeutics* **6,** 13–29. http://dx.doi.org/10.1093/abt/tbac029 (2022).
4. Mullard, A. FDA approves 100th monoclonal antibody product. *Nature Reviews Drug Discovery* **20,** 491–495. https://doi.org/10.1038/d41573-021-00079-7 (2021).
5. Jacobs, S. A., Wu, S.-J., Feng, Y., Bethea, D. & O'Neil, K. T. Cross-Interaction Chromatography: A Rapid Method to Identify Highly Soluble Monoclonal Antibody Candidates. *Pharmaceutical Research* **27,** 65–71. ISSN: 1573-904X. http://dx.doi.org/10.1007/s11095-009-0007-z (2009).
6. Fernández-Quintero, M. L. *et al.* Assessing developability early in the discovery process for novel biologics. *mAbs* **15.** http://dx.doi.org/10.1080/19420862.2023.2171248 (2023).
7. Liu, Y. *et al.* High-throughput screening for developability during early-stage antibody discovery using self-interaction nanoparticle spectroscopy. *mAbs* **6,** 483–492. https://doi.org/10.4161/mabs.27431 (2013).

8. Starr, C. G. *et al.* Ultradilute Measurements of Self-Association for the Identification of Antibodies with Favorable High-Concentration Solution Properties. *Molecular Pharmaceutics* **18,** 2744–2753. http://dx.doi.org/10.1021/acs.molpharmaceut.1c00280 (2021).
9. Khera, H. K. *et al.* Nano-differential scanning fluorimetry as a tool for the assessment of refolded antibody fragments: A case study for anti-Pfs25 single-chain antibodies. *Biochemical Engineering Journal* **206,** 109287. ISSN: 1369-703X. http://dx.doi.org/10.1016/j.bej.2024.109287 (2024).
10. Bauer, J. *et al.* How can we discover developable antibody-based biotherapeutics? *Frontiers in Molecular Biosciences* **10.** ISSN: 2296-889X. http://dx.doi.org/10.3389/fmolb.2023.1221626 (2023).
11. Gordon, G. L., Raybould, M. I. J., Wong, A. & Deane, C. M. Prospects for the computational humanization of antibodies and nanobodies. *Frontiers in Immunology* **15.** http://dx.doi.org/10.3389/fimmu.2024.1399438 (2024).
12. Chennamsetty, N., Voynov, V., Kayser, V., Helk, B. & Trout, B. L. Design of therapeutic proteins with enhanced stability. *Proceedings of the National Academy of Sciences* **106,** 11937–11942. https://doi.org/10.1073/pnas.0904191106 (2009).
13. Lauer, T. M. *et al.* Developability Index: A Rapid In Silico Tool for the Screening of Antibody Aggregation Propensity. *Journal of Pharmaceutical Sciences* **101,** 102–115. https://doi.org/10.1002/jps.22758 (2012).
14. Obrezanova, O. *et al.* Aggregation risk prediction for antibodies and its application to biotherapeutic development. *mAbs* **7,** 352–363. https://doi.org/10.1080/19420862.2015.1007828 (2015).
15. Sharma, V. K. *et al.* In silico selection of therapeutic antibodies for development: Viscosity, clearance, and chemical stability. *Proceedings of the National Academy of Sciences* **111,** 18601–18606. https://doi.org/10.1073/pnas.1421779112 (2014).
16. Agrawal, N. J. *et al.* Computational tool for the early screening of monoclonal antibodies for their viscosities. *mAbs* **8,** 43–48. https://doi.org/10.1080/19420862.2015.1099773 (2015).
17. Sydow, J. F. *et al.* Structure-Based Prediction of Asparagine and Aspartate Degradation Sites in Antibody Variable Regions. *PLoS ONE* **9** (ed Dübel, S.) e100736. https://doi.org/10.1371/journal.pone.0100736 (2014).
18. Lai, P.-K. DeepSCM: An efficient convolutional neural network surrogate model for the screening of therapeutic antibody viscosity. *Computational and Structural Biotechnology Journal* **20,** 2143–2152. http://dx.doi.org/10.1016/j.csbj.2022.04.035 (2022).
19. Kalejaye, L., Wu, I.-E., Terry, T. & Lai, P.-K. DeepSP: Deep learning-based spatial properties to predict monoclonal antibody stability. *Computational and Structural Biotechnology Journal* **23,** 2220–2229. http://dx.doi.org/10.1016/j.csbj.2024.05.029 (2024).
20. Kalejaye, L. A. *et al.* Accelerating high-concentration monoclonal antibody development with large-scale viscosity data and ensemble deep learning. *mAbs* **17.** http://dx.doi.org/10.1080/19420862.2025.2483944 (2025).
21. Waight, A. B. *et al.* A machine learning strategy for the identification of key in silico descriptors and prediction models for IgG monoclonal antibody developability properties. *mAbs* **15.** http://dx.doi.org/10.1080/19420862.2023.2248671 (2023).
22. Makowski, E. K. *et al.* Co-optimization of therapeutic antibody affinity and specificity using machine learning models that generalize to novel mutational space. *Nature Communications* **13.** http://dx.doi.org/10.1038/s41467-022-31457-3 (2022).
23. Makowski, E. K. *et al.* Optimization of therapeutic antibodies for reduced self-association and non-specific binding via interpretable machine learning. *Nature Biomedical Engineering* **8,** 45–56. ISSN: 2157-846X. http://dx.doi.org/10.1038/s41551-023-01074-6 (2023).
24. Dreyer, F. A. *et al.* Computational design of therapeutic antibodies with improved developability: efficient traversal of binder landscapes and rescue of escape mutations. *mAbs* **17.** http://dx.doi.org/10.1080/19420862.2025.2511220 (2025).
25. Ahmed, L. *et al.* Intrinsic physicochemical profile of marketed antibody-based biotherapeutics. *Proceedings of the National Academy of Sciences* **118.** https://doi.org/10.1073/pnas.2020577118 (2021).
26. Park, E. & Izadi, S. Molecular surface descriptors to predict antibody developability: sensitivity to parameters, structure models, and conformational sampling. *mAbs* **16.** http://dx.doi.org/10.1080/19420862.2024.2362788 (2024).
27. Bashour, H. *et al.* Biophysical cartography of the native and human-engineered antibody landscapes quantifies the plasticity of antibody developability. *Communications Biology* **7.** http://dx.doi.org/10.1038/s42003-024-06561-3 (2024).
28. Arras, P. *et al.* A library approach for the de novo high-throughput isolation of humanized VHH domains with favorable developability properties following camelid immunization. *mAbs* **15.** http://dx.doi.org/10.1080/19420862.2023.2261149 (2023).

29. Arras, P. *et al.* AI/ML combined with next-generation sequencing of VHH immune repertoires enables the rapid identification of de novo humanized and sequence-optimized single domain antibodies: a prospective case study. *Frontiers in Molecular Biosciences* **10.** ISSN: 2296-889X. http://dx.doi.org/10.3389/fmolb.2023.1249247 (2023).
30. Tomimoto, Y., Yamazaki, R. & Shirai, H. Increasing the melting temperature of VHH with the in silico free energy score. *Scientific Reports* **13.** http://dx.doi.org/10.1038/s41598-023-32022-8 (2023).
31. Conrath, K. *et al.* Antigen Binding and Solubility Effects upon the Veneering of a Camel VHH in Framework-2 to Mimic a VH. *Journal of Molecular Biology* **350,** 112–125. http://dx.doi.org/10.1016/j.jmb.2005.04.050 (2005).
32. Eshak, F. & Goupil-Lamy, A. Advancements in Nanobody Epitope Prediction: A Comparative Study of AlphaFold2Multimer vs AlphaFold3. *Journal of Chemical Information and Modeling* **65,** 1782–1797. ISSN: 1549-960X. http://dx.doi.org/10.1021/acs.jcim.4c01877 (2025).
33. Gordon, G. L. *et al.* A comparison of the binding sites of antibodies and single-domain antibodies. *Frontiers in Immunology* **14.** http://dx.doi.org/10.3389/fimmu.2023.1231623 (2023).
34. Raybould, M. I. J. *et al.* Thera-SAbDab: the Therapeutic Structural Antibody Database. *Nucleic Acids Research* **48,** D383–D388. https://doi.org/10.1093/nar/gkz827 (2019).
35. Kovaltsuk, A. *et al.* Observed Antibody Space: A Resource for Data Mining Next-Generation Sequencing of Antibody Repertoires. *J. Immunol* **201,** 2502–2509. http://dx.doi.org/10.4049/jimmunol.1800708 (2018).
36. Olsen, T. H., Boyles, F. & Deane, C. M. Observed Antibody Space: A diverse database of cleaned, annotated, and translated unpaired and paired antibody sequences. *Protein Science* **31,** 141–146. https://doi.org/10.1002/pro.4205 (2021).
37. Gordon, G. L. *et al.* PLAbDab-nano: a database of camelid and shark nanobodies from patents and literature. *Nucleic Acids Research.* http://dx.doi.org/10.1093/nar/gkae881 (2024).
38. Dunbar, J. *et al.* SAbDab: the structural antibody database. *Nucleic Acids Research* **42,** D1140–D1146. https://doi.org/10.1093/nar/gkt1043 (2013).
39. Schneider, C., Raybould, M. I. J. & Deane, C. M. SAbDab in the age of biotherapeutics: updates including SAbDab-nano, the nanobody structure tracker. *Nucleic Acids Research* **50,** D1368–D1372. https://doi.org/10.1093/nar/gkab1050 (2021).
40. Jaffe, D. B. *et al.* Functional antibodies exhibit light chain coherence. *Nature* **611,** 352–357. http://dx.doi.org/10.1038/s41586-022-05371-z (2022).
41. Li, X. *et al.* Comparative Analysis of Immune Repertoires between Bactrian Camel's Conventional and Heavy-Chain Antibodies. *PLOS ONE* **11** (ed Fugmann, S. D.) e0161801. https://doi.org/10.1371/journal.pone.0161801 (2016).
42. Abanades, B. *et al.* ImmuneBuilder: Deep-Learning models for predicting the structures of immune proteins. *Communications Biology* **6.** https://doi.org/10.1038/s42003-023-04927-7 (2023).
43. Lefranc, M.-P. *et al.* IMGT unique numbering for immunoglobulin and T cell receptor variable domains and Ig superfamily V-like domains. *Developmental & Comparative Immunology* **27,** 55–77. https://doi.org/10.1016/s0145-305x(02)00039-3 (2003).
44. Dunbar, J. & Deane, C. M. ANARCI: antigen receptor numbering and receptor classification. *Bioinformatics,* btv552. https://doi.org/10.1093/bioinformatics/btv552 (2015).
45. Weitzner, B. D., Dunbrack, R. L. & Gray, J. J. The Origin of CDR H3 Structural Diversity. *Structure* **23,** 302–311. http://dx.doi.org/10.1016/j.str.2014.11.010 (2015).
46. Bahrami Dizicheh, Z., Chen, I.-L. & Koenig, P. VHH CDR-H3 conformation is determined by VH germline usage. *Communications Biology* **6.** http://dx.doi.org/10.1038/s42003-023-05241-y (2023).
47. Jubb, H. C. *et al.* Arpeggio: A Web Server for Calculating and Visualising Interatomic Interactions in Protein Structures. *Journal of Molecular Biology* **429,** 365–371. https://doi.org/10.1016/j.jmb.2016.12.004 (2017).
48. Wojdyr, M. GEMMI: A library for structural biology. *Journal of Open Source Software* **7,** 4200. http://dx.doi.org/10.21105/joss.04200 (2022).
49. Schrödinger, LLC. *The PyMOL Molecular Graphics System, Version 1.8* Nov. 2015.
50. Tareen, A. & Kinney, J. B. Logomaker: beautiful sequence logos in Python. *Bioinformatics* **36** (ed Valencia, A.) 2272–2274. http://dx.doi.org/10.1093/bioinformatics/btz921 (2019).
51. Hunter, J. D. Matplotlib: A 2D Graphics Environment. *Computing in Science &amp Engineering* **9,** 90–95. https://doi.org/10.1109/mcse.2007.55 (2007).
52. Estep, P. *et al.* An alternative assay to hydrophobic interaction chromatography for high-throughput characterization of monoclonal antibodies. *mAbs* **7,** 553–561. http://dx.doi.org/10.1080/19420862.2015.1016694 (2015).
53. Muyldermans, S. *et al.* Camelid immunoglobulins and nanobody technology. *Veterinary Immunology and Immunopathology* **128,** 178–183.

https://doi.org/10.1016/j.vetimm.2008.10.299 (2009).
54. Sircar, A., Sanni, K. A., Shi, J. & Gray, J. J. Analysis and Modeling of the Variable Region of Camelid Single-Domain Antibodies. *The Journal of Immunology* **186,** 6357–6367. https://doi.org/10.4049/jimmunol.1100116 (2011).
55. Mitchell, L. S. & Colwell, L. J. Comparative analysis of nanobody sequence and structure data. *Proteins: Structure, Function, and Bioinformatics* **86,** 697–706. https://doi.org/10.1002/prot.25497 (2018).
56. Zavrtanik, U., Lukan, J., Loris, R., Lah, J. & Hadži, S. Structural Basis of Epitope Recognition by Heavy-Chain Camelid Antibodies. *Journal of Molecular Biology* **430,** 4369–4386. https://doi.org/10.1016/j.jmb.2018.09.002 (2018).
57. Soler, M. A. *et al.* Effect of Humanizing Mutations on the Stability of the Llama Single-Domain Variable Region. *Biomolecules* **11,** 163. ISSN: 2218-273X. http://dx.doi.org/10.3390/biom11020163 (2021).
58. Kuroda, D. & Tsumoto, K. in *Computer-Aided Antibody Design* 61–79 (Springer US, 2022). ISBN: 9781071626092. http://dx.doi.org/10.1007/978-1-0716-2609-2_2.
59. Kinoshita, S. *et al.* Molecular basis for thermal stability and affinity in a VHH: Contribution of the framework region and its influence in the conformation of the CDR3. *Protein Science* **31.** ISSN: 1469-896X. http://dx.doi.org/10.1002/pro.4450 (2022).
60. Sang, Z., Xiang, Y., Bahar, I. & Shi, Y. Llamanade: An open-source computational pipeline for robust nanobody humanization. *Structure* **30,** 418–429.e3. https://doi.org/10.1016/j.str.2021.11.006 (2022).
61. Ausserwöger, H. *et al.* Non-specificity as the sticky problem in therapeutic antibody development. *Nature Reviews Chemistry* **6,** 844–861. http://dx.doi.org/10.1038/s41570-022-00438-x (2022).